Magnitudes and Relative Orientation of ^{51}V Quadrupole Coupling and Anisotropic Shielding Tensors in Metavanadates and KV_3O_8 from ^{51}V MAS NMR Spectra. ^{23}Na Quadrupole Coupling Parameters for α- and β-$NaVO_3$†

Jørgen Skibsted, Niels Chr. Nielsen, Henrik Bildsøe, and Hans J. Jakobsen*

Contribution from the Department of Chemistry, University of Aarhus, DK-8000 Aarhus C, Denmark

Received March 2, 1993

Abstract: ^{51}V MAS NMR spectra, exhibiting the complete manifold of spinning sidebands (ssb's) from all seven ^{51}V ($I = {}^7/_2$) single-quantum transitions, have been obtained for a series of metavanadates (MVO_3, M = Li, Na, K, NH_4, Tl) and for KV_3O_8 employing spectral windows up to 2 MHz. These MAS NMR spectra are influenced by interactions from both the ^{51}V quadrupole coupling and chemical shielding anisotropy. Analysis of the spectra has been performed in terms of the two interactions employing a newly developed method requiring simulations and iterative fitting of the calculated to the experimental intensities of the spinning sidebands. Accurate values for all eight parameters describing the magnitude and relative orientation of the quadrupole coupling and anisotropic shielding tensors are obtained. The applicability and high performance of the method are illustrated by comparison of simulated and experimental MAS spectra, but also when ^{51}V parameters are compared to literature data determined for a few of the vanadates from static NMR and nuclear quadrupole resonance. Correlations between ^{51}V parameters and structural characteristics for the metavanadates are discussed. Furthermore, the two polymorphs α- and β-$NaVO_3$ along with a commercial sample of sodium metavanadate (consisting of a mixture of these polymorphs) are characterized by ^{23}Na MAS NMR and the ^{23}Na quadrupole coupling parameters and isotropic chemical shifts determined from these spectra.

Introduction

High-resolution solid-state NMR spectroscopy of quadrupolar nuclei ($I > {}^1/_2$) in powders has gained widespread success in a variety of branches of solid-state chemistry and materials science during recent years. Important information about the local electronic structure and geometry around the quadrupole nucleus is provided by the quadrupole coupling constant (C_Q) and the associated asymmetry parameter (η_Q), which nowadays may conveniently be determined by using various solid-state NMR techniques. For example, C_Q reflects the distortion of the coordination polyhedron for the quadrupole nucleus[1,2] while η_Q is related to the symmetry at the nuclear site. Thus, the quadrupole coupling parameters represent an important supplement to the chemical shielding anisotropy (CSA: δ_σ and η_σ) and the more commonly reported isotropic chemical shift (δ_{iso}), i.e., parameters which are related to the net atomic charge and thereby the local electronic structure and coordination state of the atom.[3] Among the sample spinning NMR techniques, standard magic-angle spinning (MAS)[4] experiments have proven useful for extracting values for quadrupole coupling parameters and isotropic chemical shifts (corrected for second-order quadrupolar-induced shifts). Especially high-speed MAS experiments employing spinning frequencies ν_r = 18–20 kHz have proven useful since quadrupole coupling constants as large as 15–18 MHz for $I = {}^5/_2$ nuclei may be obtained from simulation of the second-order quadrupolar line shape observed for the $({}^1/_2, -{}^1/_2)$ central transition.[5-7] For smaller quadrupole interactions where the central transition does not show a well-resolved second-order line shape, accurate values for C_Q and η_Q may conveniently be determined from simulation of the intensities for the MAS NMR manifold of spinning sidebands (ssb's) observed for the satellite transitions, which are influenced by the much larger first-order quadrupolar interaction.[8,9]

Until recently MAS NMR studies of quadrupolar nuclei have been confined to spins which are almost exclusively dominated by the quadrupole interaction. Less attention has been paid to the large number of quadrupolar nuclei (e.g., ^{51}V, ^{59}Co, ^{87}Rb, and ^{95}Mo) for which CSA represents a significant additional contribution to the anisotropic interactions. The main reason for this has most likely been the lack of numerical methods for a correct interpretation of the rather complex MAS NMR spectra for these nuclei. Recently, we demonstrated that observation of the complete manifold of ssb's from all seven ^{51}V ($I = {}^7/_2$) single-quantum transitions in ^{51}V MAS NMR spectra represent an efficient mean for accurate determination of the parameters for the quadrupole coupling (C_Q, η_Q) and CSA (δ_σ, η_σ, and δ_{iso}) tensors along with the relative orientation (ψ,χ,ξ) of their principal-axis systems.[10] We note that the combined effect from the quadrupole and CSA interactions has previously been studied by static powder[11-17] and single-crystal[18] NMR methods, however, in some

† Presented in part at the 33rd Experimental NMR Conference, Asilomar, CA, March 1992, and the XXVI Congress Ampere on Magnetic Resonance, Athens, Greece, September 1992.

(1) Edwards, J. C.; Zubieta, J.; Shaikh, S. N.; Chen, Q.; Bank, S.; Ellis, P. D. *Inorg. Chem.* **1990**, *29*, 3381.
(2) Ghose, S.; Tsang, T. *Am. Mineral.* **1973**, *58*, 748.
(3) Engelhardt, G.; Michel, D. *High Resolution Solid State NMR of Silicates and Zeolites*; John Wiley & Sons: Chichester, England, 1987.
(4) Andrew, E. R.; Bradbury, A.; Eades, R. G. *Arch. Sci.* **1958**, *11*, 223. Lowe, I. J. *Phys. Rev. Lett.* **1959**, *2*, 285.
(5) Skibsted, J.; Bildsøe, H.; Jakobsen, H. J. *J. Magn. Reson.* **1991**, *92*, 669.
(6) Dec, S. F.; Fitzgerald, J. J.; Frye, J. S.; Shatlock, M. P.; Maciel, G. E. *J. Magn. Reson.* **1991**, *93*, 403.
(7) Alemany, L. B.; Massiot, D.; Sherriff, B. L.; Smith, M. E.; Taulelle, F. *Chem. Phys. Lett.* **1991**, *177*, 301.
(8) Jakobsen, H. J.; Skibsted, J.; Bildsøe, H.; Nielsen, N. C. *J. Magn. Reson.* **1989**, *85*, 173.
(9) Skibsted, J.; Nielsen, N. C.; Bildsøe, H.; Jakobsen, H. J. *J. Magn. Reson.* **1991**, *95*, 88.
(10) Skibsted, J.; Nielsen, N. C.; Bildsøe, H.; Jakobsen, H. J. *Chem. Phys. Lett.* **1992**, *188*, 405.
(11) Baugher, J. F.; Taylor, P. C.; Oja, T.; Bray, P. J. *J. Chem. Phys.* **1969**, *50*, 4914.
(12) Cheng, J. T.; Edwards, J. C.; Ellis, P. D. *J. Phys. Chem.* **1990**, *94*, 553.
(13) Power, W. P.; Wasylishen, R. E.; Mooibroek, S.; Pettitt, B. A.; Danchura, W. *J. Phys. Chem.* **1990**, *94*, 591.
(14) France, P. W. *J. Magn. Reson.* **1991**, *92*, 30.
(15) Eckert, H.; Wachs, I. E. *J. Phys. Chem.* **1989**, *93*, 6796.
(16) Hirshinger, J.; Granger, P.; Rosé, J. *J. Phys. Chem.* **1992**, *96*, 4815.

0002-7863/93/1515-7351$04.00/0

cases assuming coincidence of the principal-axis systems for the two tensors.[11]

In this work we investigate a series of metavanadates ($LiVO_3$, α-$NaVO_3$, β-$NaVO_3$, KVO_3, NH_4VO_3, and $TlVO_3$) as well as KV_3O_8 using ^{51}V MAS NMR. This includes the first determination of all eight parameters (i.e., C_Q, η_Q, δ_σ, η_σ, δ_{iso}, ψ, χ, and ξ), describing the magnitudes and relative orientation of the quadrupole coupling and anisotropic shielding tensors, from simulation and iterative fitting of the manifolds of ssb's observed over spectral widths up to 2 MHz. It is demonstrated that ^{51}V MAS NMR allows determination of these parameters for the metavanadates with improved accuracy compared to those obtained with static NMR methods.[11,15,17] Furthermore, it is illustrated that ^{51}V MAS NMR enable qualitative and quantitative discrimination of a mixture of the α-$NaVO_3$ and β-$NaVO_3$ polymorphs as observed for a commercial sample of sodium metavanadate. Alternatively, information about the polymorph composition of this mixture can be obtained using ^{23}Na MAS NMR and ^{23}Na quadrupole coupling parameters and isotropic chemical shifts are determined for the α- and β-$NaVO_3$ phases. The applicability of ^{51}V MAS NMR for samples containing more than one vanadium site in the asymmetric unit is illustrated by the spectrum of KV_3O_8. The ^{51}V quadrupole coupling parameters for KVO_3, NH_4VO_3, and α-$NaVO_3$ are compared with those obtained in a recent nuclear quadrupole resonance (NQR) study by Mao et al.,[19] where it is claimed that accurate C_Q and η_Q values for ^{51}V may hardly be determined by solid-state NMR methods.

Theory

In the secular approximation the time-domain signal resulting from a single-pulse ^{51}V MAS NMR experiment may be described (assuming ideal excitation) as

$$s(t) = \sum_{\alpha\beta\gamma} \sum_{m} p_m \exp\{i \int_0^t [\langle m|\tilde{\mathcal{H}}(t')|m\rangle - \langle m-1|\tilde{\mathcal{H}}(t')|m-1\rangle]\, dt'\} \quad (1)$$

where $p_m = I(I+1) - m(m-1)$ denotes the squared $(m, m-1)$ transition probability ($m = -I+1, \ldots, I$) and $\tilde{\mathcal{H}}(t)$ the combined quadrupole and anisotropic shielding average Hamiltonian in the Zeeman interaction representation. To first order in the average Hamiltonian approximation $\tilde{\mathcal{H}}(t)$ takes the form

$$\tilde{\mathcal{H}}(t) = \sum_{k=-2}^{2} \{\omega_Q^{(k)}[3I_z^2 - I(I+1)] + \omega_\sigma^{(k)} I_z\} \exp(ik\omega_r t) \quad (2)$$

where $\omega_r/2\pi = \nu_r$ denotes the spinning frequency and $\omega_\lambda^{(k)}$ the orientationally-dependent Fourier components for the quadrupole ($\lambda = Q$) and shielding ($\lambda = \sigma$) interactions. The Fourier components may be expressed as

$$\omega_\lambda^{(k)} = \omega_\lambda^{iso}\delta_{k,0} + \omega_\lambda \left\{ D_{0,-k}^2(\Omega_{PR}^\lambda) - \frac{\eta_\lambda}{\sqrt{6}}[D_{-2,-k}^2(\Omega_{PR}^\lambda) + D_{2,-k}^2(\Omega_{PR}^\lambda)] \right\} d_{0,-k}^2(\beta_{RL}) \quad (3)$$

where $\omega_Q = 2\pi C_Q/\{4I(2I-1)\}$, $\omega_\sigma = \omega_0\delta_\sigma$, $\omega_0 = -\gamma B_0$, and $0 \le \eta_\lambda \le 1$; only the shielding interaction has an isotropic component $\omega_\sigma^{iso} = \omega_0\delta_{iso}$ ($\delta_{k,0}$ is a Kronecker delta and $\omega_0/2\pi = \nu_0$, the resonance frequency). $D_{k,l}^2$ is a Wigner matrix element and $\Omega_{PR}^\lambda = \{\alpha,\beta,\gamma\}$ are the Euler angles[20] relating the rotor-fixed frame (R) to the principal-axis frame (P^λ) of the interaction λ. The principal-axis frame for the anisotropic shielding tensor (P^σ) is related to P^Q through an additional Wigner rotation with Euler angles (ψ,χ,ξ), i.e., $D^2(\Omega_{PR}^Q) = D^2(\alpha,\beta,\gamma)$ and $D^2(\Omega_{PR}^\sigma) = D^2(\alpha,\beta,\gamma)D^2(\psi,\chi,\xi)$. $d_{k,l}^2$ is a reduced Wigner element relating R to the laboratory frame (L), where $\beta_{RL} = \tan^{-1}(1/\sqrt{2})$ under MAS conditions. Explicit expressions describing the transformation of the CSA tensor from P^σ into P^Q followed by transformation of both tensors to the laboratory-fixed frame via the R frame have recently been presented.[10] The symmetry of these expressions reduces the ranges of the Euler angles relating the CSA and quadrupole tensors to $0 \le \psi, \chi, \xi \le \pi$. Summation over all uniformly distributed crystallite orientations (i.e., averaging of the α, β, γ angles) introduces new symmetry relations for the time domain signal:

$$s(t;\psi,\chi,\xi) = s(t;\pi-\psi,\chi,\pi-\xi) = s(t;\pi-\psi,\pi-\chi,\xi) = s(t;\psi,\pi-\chi,\pi-\xi) \quad (4)$$

implying that the ranges for the Euler angles can be limited to the intervals $0 \le \psi \le \pi$ and $0 \le \chi, \xi \le \pi/2$. The interaction parameters are expressed by the principal elements of the shielding (σ) and electric field-gradient (EFG, V) tensors using the standard convention[20] $|\lambda_{zz} - {}^1/_3\mathrm{Tr}(\lambda)| \ge |\lambda_{xx} - {}^1/_3\mathrm{Tr}(\lambda)| \ge |\lambda_{yy} - {}^1/_3\mathrm{Tr}(\lambda)|$ for $\lambda = \sigma$, V, i.e.,

$$\delta_\sigma = \sigma_{zz} - {}^1/_3\mathrm{Tr}(\sigma),\ \eta_\sigma = (\sigma_{yy} - \sigma_{xx})/\delta_\sigma,\quad C_Q = \frac{eQ}{h}V_{zz},\quad \eta_Q = (V_{yy} - V_{xx})/V_{zz} \quad (5)$$

A simulation program, based on the above formalism and combined with the nonlinear optimization package MINUIT,[21] has been designed for iterative fitting to the experimental ssb intensities in order to determine accurate values for the seven parameters (C_Q, η_Q, δ_σ, η_σ, ψ, χ, ξ) describing the magnitudes and relative orientations of the ^{51}V quadrupole and anisotropic shielding tensors. The isotropic chemical shift (δ_{iso}) is determined from the center of gravity of the centerband for the $({}^1/_2, -{}^1/_2)$ transition taking the second-order quadrupolar shift into account.

Experimental Section

^{51}V and ^{23}Na MAS NMR spectra were obtained on Varian XL-300 (7.1 T), VXR-400 S (9.4 T), and UNITY-500 (11.7 T) spectrometers all equipped with homebuilt MAS probes[22] for 7 mm o.d. rotors allowing spinning speeds up to 10 kHz (Si_3N_4 rotors) with a stability of ± 5 Hz to be employed. All experiments used single-pulse excitation with a pulse width of $\tau_p = 1$ μs, a rf field strength of $\gamma H_1/2\pi \approx 50$ kHz, and a 1-s relaxation delay. The isotropic chemical shifts, reported in ppm and corrected for second-order quadrupolar induced shifts, are relative to external samples of neat $VOCl_3$ (^{51}V) and 1.0 M NaCl (^{23}Na). The δ scale is positive toward lower shielding whereas the principal elements of the shielding tensor (σ_{ii}) are positive in the opposite direction ($\sigma = -\delta$). A 0.16 M $NaVO_3$ aqueous solution was used as a secondary reference sample for the ^{51}V MAS NMR spectra. The isotropic chemical shift value of $\delta_{iso} = -574.38$ ppm determined for this solution relative to neat $VOCl_3$ is in excellent agreement with an earlier reported value ($\delta_{iso} = -574.28$ ppm).[17] In all figures, the kHz scale is referenced to the center of gravity for the isotropic peak, as determined from spectra employing different spinning speeds. Simulations were performed on a Digital VAX-6210 computer with the software described elsewhere.[9,10]

The samples for KVO_3, NH_4VO_3, and $NaVO_3$ were obtained commercially and their MAS NMR spectra recorded without further purification. However, ^{51}V and ^{23}Na MAS NMR spectra as well as an X-ray powder diffraction (XRD) diagram of sodium metavanadate revealed that this sample is composed of a mixture of the α- and β-$NaVO_3$ polymorphs. From the commercial $NaVO_3$ product, α-$NaVO_3$ was

(17) Hayashi, S.; Hayamizu, K. *Bull. Chem. Soc. Jpn.* **1990**, *63*, 961.
(18) Gornostansky, S. D.; Stager, C. V. *J. Chem. Phys.* **1967**, *46*, 4959.
(19) Mao, D.; Bray, P. J.; Petersen, G. L. *J. Am. Chem. Soc.* **1991**, *113*, 6812.
(20) Spiess, H. W. In *NMR Basic Principles and Progress*; Diehl, P., Fluck, E., Kosfeld, E.; Springer: Berlin, 1978; Vol. 15.
(21) James, F.; Ross, M. "MINUIT Computer Code", CERN, Geneva, Program D-506; *Comput. Phys. Comm.* **1975**, *10*, 343.
(22) Jakobsen, H. J.; Daugaard, P.; Langer, V. *J. Magn. Reson.* **1988**, *76*, 162; U.S. Patent Number 4,739,270, April 19, 1988.

Table I. ^{51}V Quadrupole Couplings (C_Q,η_Q), Chemical Shielding Anisotropies (δ_σ,δ_σ), Relative Orientation of the Principal Axis Systems (ψ,χ,ξ) for the Quadrupole Coupling and Chemical Shielding Anisotropy, and Isotropic Chemical Shifts (δ_{iso}) for a Series of Metavanadates and KV_3O_8 as well as ^{23}Na Quadrupole Coupling Parameters and Isotropic Chemical Shifts for α-$NaVO_3$ and β-$NaVO_3$

compound	method	C_Q (MHz)	η_Q	δ_σ[a] (ppm)	η_σ[a]	ψ[b] (deg)	χ[b] (deg)	ξ[b] (deg)	δ_{iso}[c] (ppm)	ref
^{51}V data										
$LiVO_3$	MAS NMR[d]	3.18 ± 0.07	0.87 ± 0.03	221 ± 5	0.70 ± 0.03	154 ± 10	9 ± 10	4 ± 10	−573.4 ± 0.5[e]	this work
	static NMR[f,g]			217 ± 23	0.69 ± 0.15				−577.1 ± 0.5	17
KVO_3	MAS NMR[d]	4.20 ± 0.10	0.80 ± 0.05	290 ± 5	0.65 ± 0.03	90 ± 10	0 ± 10	31 ± 10	−552.7 ± 0.5[e]	this work
	single crystal NMR	4.22 ± 0.15	0.65 ± 0.15							31
	static NMR[g,h]	4.36 ± 0.06	0.75 ± 0.10	227 ± 23	0.88 ± 0.15					11
	static NMR[g,i]			313 ± 12	0.64 ± 0.05				−553 ± 2	15
	static NMR[f,g]			303 ± 23	0.63 ± 0.10				−557.7 ± 0.5	17
	NQR[j]	4.201 ± 0.002	0.794 ± 0.001							19
NH_4VO_3	MAS NMR[k]	2.95 ± 0.07	0.30 ± 0.03	240 ± 5	0.70 ± 0.03	78 ± 10	23 ± 7	32 ± 10	−569.5 ± 0.5[e]	this work
	MAS NMR[d]	2.91 ± 0.07	0.30 ± 0.03	237 ± 5	0.71 ± 0.03	75 ± 10	23 ± 7	34 ± 10	−569.0 ± 0.5[e]	10
	static NMR[g,h]	2.88 ± 0.06	0.30 ± 0.10	250 ± 23	0.28 ± 0.12					11
	static NMR[g,i]			253 ± 12	0.63 ± 0.06				−570 ± 2	15
	static NMR[f,g]			243 ± 23	0.62 ± 0.13				−571.5 ± 0.5	17
	NQR[j]	2.975 ± 0.020	0.437 ± 0.020							19
$TlVO_3$	MAS NMR[d]	3.67 ± 0.10	0.71 ± 0.04	265 ± 5	0.76 ± 0.03	114 ± 10	21 ± 7	4 ± 10	−529.1 ± 0.5[e]	this work
α-$NaVO_3$	MAS NMR[d]	3.80 ± 0.10	0.46 ± 0.04	259 ± 5	0.68 ± 0.03	30 ± 10	15 ± 10	15 ± 10	−572.7 ± 0.5[e]	this work
	static NMR[g,h]	3.65 ± 0.06	0.60 ± 0.10	253 ± 23	0.87 ± 0.14					11
	static NMR[g,i]			269	0.58					33
	static NMR[g,i]			263 ± 12	0.65 ± 0.06				−576 ± 2	15
	static NMR[f,g]			253 ± 23	0.63 ± 0.13				−578.2 ± 0.5	17
	NQR[j]	3.745 ± 0.003	0.489 ± 0.003							19
β-$NaVO_3$	MAS NMR[d]	4.20 ± 0.10	0.55 ± 0.04	512 ± 7	0.17 ± 0.05	177 ± 15	48 ± 5	9 ± 10	−510.4 ± 0.5[e]	this work
	static NMR[f,g]			507 ± 20	0.00 ± 0.08				−516.4 ± 0.5	17
KV_3O_8 V(1)	MAS NMR[d]	2.45 ± 0.10	0.44 ± 0.03	405 ± 5	0.00 ± 0.07	—[l]	65 ± 5	90 ± 7	−548.1 ± 0.5[e]	this work[l]
V(2)	MAS NMR[d]	3.03 ± 0.10	0.89 ± 0.03	459 ± 5	0.00 ± 0.07	—[l]	61 ± 7	56 ± 7	−510.0 ± 0.5[e]	this work[l]
^{23}Na data										
α-$NaVO_3$ Na(1)	MAS NMR	1.50 ± 0.05	0.58 ± 0.02						−15.6 ± 0.5[e]	this work
Na(2)	MAS NMR	0.765 ± 0.020	0.06 ± 0.02						−4.8 ± 0.2[e]	this work
β-$NaVO_3$	MAS NMR	1.42 ± 0.02	0.27 ± 0.02						−10.3 ± 0.3[e]	this work

[a] The CSA parameters are defined as follows: $\delta_\sigma = \sigma_{zz} - {}^1/_3\mathrm{Tr}(\sigma)$, $\eta_\sigma = (\sigma_{yy} - \sigma_{xx})/\delta_\sigma$, where the principal elements of the CSA tensor fulfill $|\sigma_{zz} - {}^1/_3\mathrm{Tr}(\sigma)| \geq |\sigma_{xx} - {}^1/_3\mathrm{Tr}(\sigma)| \geq |\sigma_{yy} - {}^1/_3\mathrm{Tr}(\sigma)|$. [b] Euler angles relating the principal axis systems for the quadrupole coupling and CSA tensors. [c] Isotropic chemical shifts on the δ scale are referenced to liquid $VOCl_3$ (^{51}V) and 1.0 M NaCl (^{23}Na). [d] Optimized ^{51}V data from ^{51}V MAS NMR spectra at 9.4 T. Uncertainty limits are estimated from the RMS deviation between experimental and simulated ssb intensities in combination with separate simulations where only one parameter is varied. [e] δ_{iso} corrected for the second-order quadrupolar shift. [f] δ_σ and η_σ determined from static NMR and δ_{iso} from MAS NMR. [g] Values calculated from the principal elements of the CSA tensor with use of the expressions in footnote *a*. [h] Parameters from static NMR at low magnetic field. [i] CSA data determined from static NMR spectra of the central transition assuming the line shape to be dominated by the CSA interaction at high magnetic fields. [j] Data from NQR at 300 K. [k] Optimized ^{51}V data from a ^{51}V MAS NMR spectrum recorded at 11.7 T with uncertainty limits determined as in footnote *d*. [l] For $\eta_\sigma = 0$ the ψ angle becomes undefined.

obtained by heating the sample overnight at 450 °C.[23] Dissolution of the commercial mixture of sodium metavanadate in water at ca. 70 °C resulted in precipitation of crystals of the hydrate β-$NaVO_3$·xH_2O after storage of the solution at room temperature for ca. 10 weeks. Anhydrous β-$NaVO_3$ was obtained by heating the hydrate at 300 °C for 2 days. $LiVO_3$ and $TlVO_3$ were prepared by reaction of lithium and thallium carbonate with V_2O_5 following the procedure reported elsewhere.[23] KV_3O_8 was kindly provided by Dr. K. West, who recently reported the synthesis of this compound.[24] The basic structure and purity of all samples were checked by XRD.

Results and Discussion

The crystal structures of the metavanadates MVO_3 (M = Li, Na, K, NH_4, Tl) all contain infinite chains of corner-sharing VO_4 tetrahedra with a single vanadium site in the asymmetric unit.[25-28] KVO_3, NH_4VO_3, and $TlVO_3$ have orthorhomic lattices (space group *Pbcm*),[25,26] while $LiVO_3$ and α-$NaVO_3$ are isomorphous compounds with a monoclinic structure (space group $C2/c$).[27,28] The low-temperature β form of $NaVO_3$ has an orthorhombic structure (space group *Pnma*)[29] with vanadium coordinated to five oxygens in distorted trigonal-bipyramidal units. α-$NaVO_3$ contains two Na sites in the asymmetric unit while all Na atoms are equivalent in β-$NaVO_3$. KV_3O_8 consists of layers of highly distorted VO_6 octahedra linked together by sharing corners and edges. The monoclinic structure (spacegroup $P2_1/m$)[30] for KV_3O_8 contains two nonequivalent vanadium atoms in the asymmetric unit in a ratio of 1:2.

The applicability of ^{51}V MAS NMR for determination of the magnitudes and relative orientation of the ^{51}V quadrupole and CSA tensors from integrated ssb intensities of all seven ^{51}V single-quantum transitions is demonstrated below for the above-mentioned metavanadates and KV_3O_8. The accuracy and performance of the method is compared with that of other methods such as ^{51}V static-sample NMR and NQR. Methods for obtaining estimates of C_Q, δ_σ, and η_σ, required as input to the optimization software, are demonstrated for $LiVO_3$. Effects from the second-order quadrupolar contribution to the effective Hamiltonian are illustrated for KVO_3 and $TlVO_3$. The effects of the relative magnitude of the CSA and quadrupole coupling on the ^{51}V MAS NMR spectra, observed at different magnetic field strengths, are illustrated for NH_4VO_3. The performance of the method for samples containing nonequivalent vanadium sites is illustrated by the ^{51}V MAS NMR spectrum of KV_3O_8. ^{51}V and ^{23}Na MAS

(23) Feigelson, R. S.; Martin, G. W.; Johnson, B. C. *J. Cryst. Growth* **1972**, *13/14*, 686.
(24) West, K.; Zachau-Christiansen, B.; Jacobsen, T.; Skaarup, S. *Solid State Ionics* **1990**, *40*, 585.
(25) Evans, H. T. *Z. Kristallogr.* **1960**, *114*, 257.
(26) Ganne, M.; Piffard, Y.; Tournoux, M. *Can. J. Chem.* **1974**, *52*, 3539.
(27) Shannon, R. D.; Calvo, C. *Can. J. Chem.* **1973**, *51*, 265.
(28) Marumo, F.; Isobe, M.; Iwai, S.; Kondo, Y. *Acta Crystallogr.* **1974**, *B30*, 1628.
(29) Kato, K.; Takayama, E. *Acta Crystallogr.* **1984**, *B40*, 102.
(30) Evans, H. T.; Block, S. *Inorg. Chem.* **1966**, *5*, 1808.

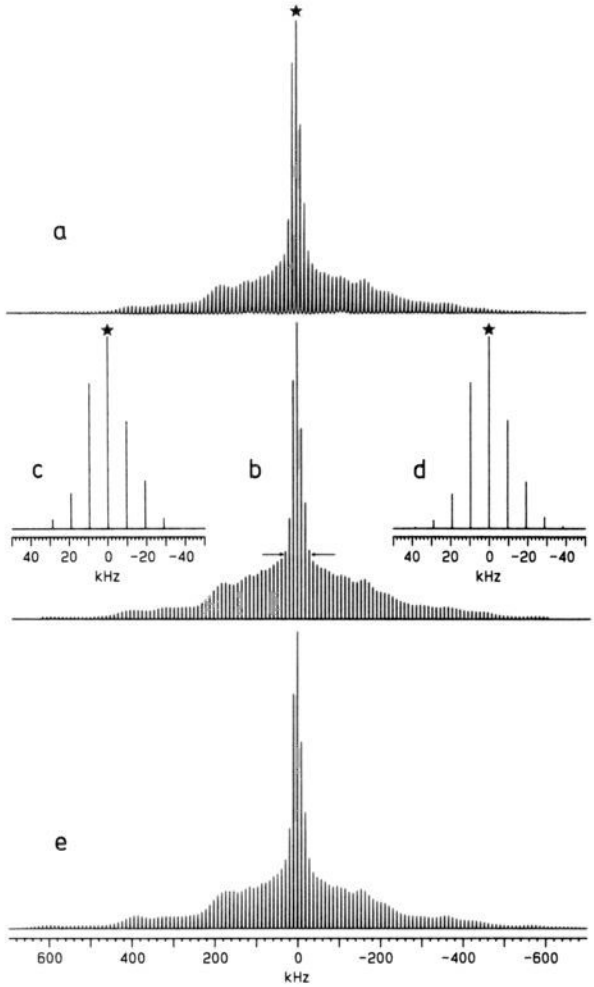

Figure 1. ^{51}V MAS NMR spectrum (105.15 MHz) of the central and satellite transitions for $LiVO_3$. (a) Experimental spectrum (ν_r = 9.6 kHz). (b) Stick-plot of 128 integrated ssb intensities for the spectrum in part a. (c) Stick-plot of approximate ssb intensities for the central transition obtained from part b as the intensities of the ssb's above the arrows. (d) Simulated ssb intensities (stick-plot) for the central transition obtained from optimization of a CSA ssb pattern to the ssb intensities in part c and corresponding to the values δ_σ = 230 ppm and η_σ = 0.75 (initial values for the seven-parameter fit, see text). (e) Simulated MAS spectrum corresponding to the optimized parameters in Table I and resulting from a seven-parameter fit of the 128 ssb intensities in part b. A Gaussian line width of 1000 Hz has been employed for the ssb's in part e. The asterisk indicates the isotropic peak.

NMR spectra of α- and β-$NaVO_3$ demonstrate that structural information can be obtained for these samples and that quantitative analysis for a mixture of the two polymorphs is possible with either nuclei. Finally, the relation between ^{51}V NMR data and crystal structure is discussed. The ^{51}V and ^{23}Na parameters determined in this work and previous studies are summarized and compared in Table I.

$LiVO_3$. The ^{51}V MAS NMR spectrum of $LiVO_3$, recorded at 9.4 T with a spinning speed of ν_r = 9.6 kHz, is shown in Figure 1a and illustrates the observation of the complete manifold of ssb's extending over a spectral width of about 1.4 MHz from all seven ^{51}V single-quantum transitions. The centerbands and ssb's from the individual transitions overlap heavily and only minor variations in the line widths of the ssb's are observed over the full spectral range. Optimum advantage of the spectral information is obtained by employing our simulation software for a seven-parameter fit. In addition to the integrated ssb intensities (Figure 1b), the optimization routine requires estimates of the ^{51}V parameters as input. A fair estimate of C_Q may be obtained from the total width ($6\nu_Q = 18C_Q/\{2I(2I-1)\}$) of the ssb manifold since the outer ($\pm^7/_2, \pm^5/_2$) transitions to a good approximation are only influenced by the quadrupolar interaction. This is due to the fact that the effect of the CSA relative to the quadrupole interaction decreases considerably (proportional to $|\delta_\sigma\omega_0/[\omega_Q(6m-3)]|$) with increasing $|m|$ quantum number for the transitions.[10] For $LiVO_3$ the ssb's are observed over a spectral range of ca. 1.4 MHz which gives the estimated value of $C_Q \approx$ 3.3 MHz. The CSA parameters are estimated by fitting the most intense ssb's from the central transition (unperturbed by the quadrupole interaction to first order) to a pure CSA pattern. Approximate ssb intensities for the central transition (Figure 1c) are obtained from the stick-plot of integrated ssb intensities shown in Figure 1b and have been taken as the intensities of the ssb's above the height indicated by the arrows. A fit of the ssb intensities in Figure 1c to a CSA pattern provides the ssb spectrum shown in Figure 1d corresponding to the approximate values of $\delta_\sigma \approx 230$ ppm and $\eta_\sigma \approx 0.75$. Employing the estimated C_Q, δ_σ, and η_σ values as input in a least-squares fitting of simulated to integrated ssb intensities gives the optimum simulated spectrum shown in Figure 1e, which is in excellent agreement with the stick-plot of integrated ssb intensities in Figure 1b. The corresponding parameters for $LiVO_3$ are listed in Table I along with their estimated errors as obtained by the least-squares optimization and separate simulations. The CSA parameters determined from the complete ssb manifold are consistent with those reported recently for $LiVO_3$ (Table I) from static-powder NMR of the central transition assuming the line shape to be dominated by the CSA interaction at high magnetic fields.[17] In that work δ_{iso} = -577.1 ± 0.5 ppm[17] was determined from the isotropic peak in a ^{51}V MAS NMR spectrum at 9.4 T, however, without taking the second-order quadrupolar-induced shift of the central transition into account. The C_Q and η_Q values determined here from Figure 1 give a second-order quadrupolar shift of 2.9 ppm for the central transition at 9.4 T. Taking this shift into account, the isotropic chemical shift reported earlier[17] agrees with the value $\delta_{iso} = -573.4 \pm 0.5$ ppm determined in this work.

KVO_3. The ^{51}V MAS NMR spectrum of KVO_3, recorded at 9.4 T with a spectral width of 2 MHz and ν_r = 9.3 kHz, is shown in Figure 2a. The line width of the ssb's varies from ca. 1100 to 1400 Hz over the spectral range and therefore the spectrum in Figure 2a gives an imperfect impression of the intensity distribution over the ssb manifold. For visual comparison with spectra simulated by using the first-order approximation (i.e., without including second-order line shapes for the ssb's), a stick-plot of integrated experimental ssb intensities is shown in Figure 2b. Estimates of C_Q, δ_σ, and η_σ are determined as described for $LiVO_3$, and the optimum parameters resulting from iterative fitting to the 141 ssb intensities are listed in Table I. The quality of the ^{51}V parameters obtained for KVO_3 may be appreciated by comparison of the simulated ssb intensities in Figure 2c with the experimental ssb stick-plot intensities (Figure 2b). A simulated spectrum, employing the same parameters as for Figure 2c but including second-order quadrupolar-induced shifts of the individual transitions, is shown in Figure 2d. For KVO_3 these shifts (at 9.4 T) are 2280, 730, −210, and −520 Hz for the ($\pm^7/_2, \pm^5/_2$), ($\pm^5/_2, \pm^3/_2$), ($\pm^3/_2, \pm^1/_2$), and ($^1/_2, -^1/_2$) transitions, respectively. The appearance of the simulated ssb manifold in Figure 2d is in excellent agreement with the experimental spectrum (Figure 2a), which indicates that the observed variation in the line width of the ssb's is mainly caused by the overlap of second-order quadrupolar shifted ssb's from the individual transitions. A variation in line width of the ssb's from the individual transitions is expected theoretically if the line shape of the ssb's results exclusively from second-order quadrupolar effects.[32] However, the relatively large line widths observed in the experimental spectrum reveals that mechanisms other than second-order qudrupole broadening contribute significantly to the line width.

(31) Gornostansky, S. D.; Stager, C. V. *J. Chem. Phys.* **1968**, *48*, 1416.

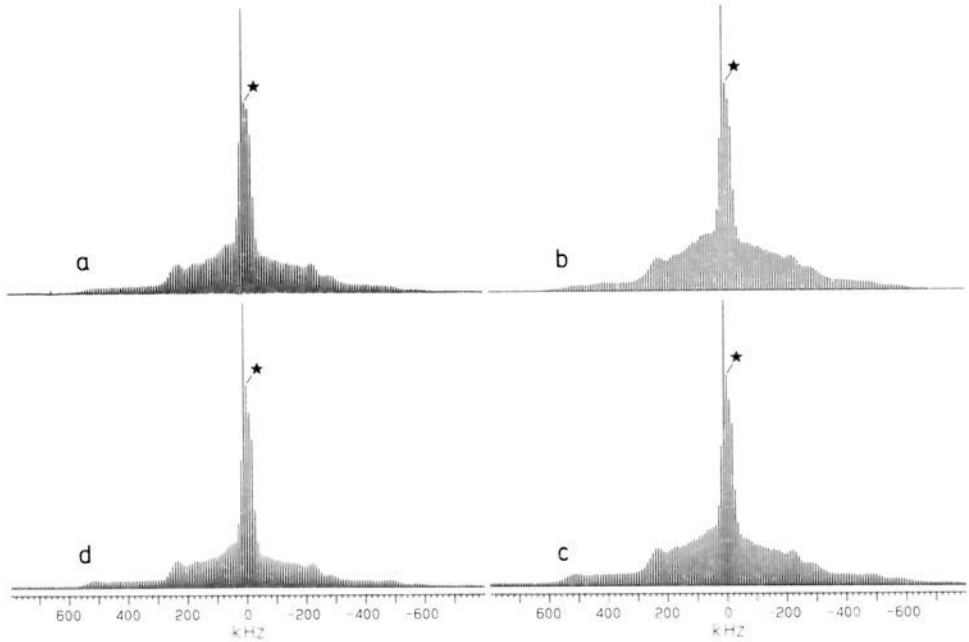

Figure 2. ^{51}V MAS NMR (105.15 MHz) spectrum of the central and satellite transitions for KVO_3. (a) Experimental spectrum (ν_r = 9.3 kHz). (b) Stick-plot of integrated ssb intensities for the spectrum in part a. (c) Simulated spectrum corresponding to the ^{51}V parameters (Table I) obtained from an optimization to the ssb's in part b; a Gaussian line width of 1000 Hz has been employed for all ssb's. (d) Simulated spectrum illustrating the same ^{51}V data as in part c but including the second-order quadrupolar shifts (see text) and Gaussian line widths of 1000 Hz ($^1/_2$, $^{-1}/_2$), 1000 Hz ($\pm^3/_2$, $\pm^1/_2$), 1200 Hz ($\pm^5/_2$, $\pm^3/_2$), and 1500 Hz ($\pm^7/_2$, $\pm^5/_2$) for the indivudal ^{51}V transitions. The isotropic peak is marked by an asterisk.

The quadrupole coupling parameters obtained from the ^{51}V MAS NMR spectra in Figure 2 agree favorably with previously reported single-crystal ^{51}V NMR data[31] and recent results from a NQR study[19] (Table I). Furthermore, ^{51}V CSA parameters for KVO_3 have been determined from static-powder spectra of the central transition at high magnetic fields[15,17] (Table I), and these values are in good agreement with the data from ^{51}V MAS NMR taking the error limits into account. Assuming coincidence of the principal axis for the CSA and quadrupole tensors, Baugher et al.[11] reported values for the magnitudes of these tensors (Table I) from line shape analysis of the central transition in a low-field static ^{51}V NMR spectrum. Comparison of these data with those obtained from the ^{51}V MAS NMR spectrum (Figure 2) clearly demonstrates the invalidity of this assumption.

NH_4VO_3. Data for the ^{51}V quadrupole coupling and CSA parameters, determined from the ^{51}V MAS NMR spectrum of NH_4VO_3 at 9.4 T, have been reported in our preliminary communication on ^{51}V MAS NMR.[10] To illustrate the field dependence of the appearance of the ssb manifold on the relative scaling of the quadrupole and CSA interactions (e.g., $\delta_\sigma\omega_0/\omega_Q$ = 0.72 and 0.90 at magnetic field strengths of 9.4 and 11.7 T, respectively, as obtained from our data determined for NH_4VO_3 at 9.4 T), Figure 3a shows the 11.7 T ^{51}V MAS NMR spectrum of NH_4VO_3 with ν_r = 9.0 kHz. Least-squares optimization of simulated to integrated ssb intensities in Figure 3b gives the ^{51}V parameters summarized in Table I. Within error limits the parameters determined at 11.7 T agree with those obtained at 9.4 T (see Table I) and serve to illustrate the reliability and accuracy of the MAS ssb method. The simulated ssb manifold corresponding to the optimized parameters at 11.7 T (Figure 3c) shows an excellent agreement with the experimental ssb intensities. The CSA parameters for NH_4VO_3 may be compared with those determined earlier from static-powder spectra of the central transition at high magnetic fields[15,17] and the quadrupole coupling parameters with those determined from NQR[19] (see Table I). Furthermore, assuming coincidence of the principal-axis frames for the two tensorial interactions, Baugher et al.[11] also reported parameters for the magnitudes of the CSA and quadrupole tensors in NH_4VO_3 (Table I). Again the invalidity of this approximation is demonstrated by comparison with our data.

$TlVO_3$. The ^{51}V MAS NMR spectrum of $TlVO_3$ (9.4 T, ν_r = 9.1 kHz) shown in Figure 4a represents the basis for the first ^{51}V NMR study of this compound. As illustrated by the insets in Figure 4a, the difference in second-order quadrupolar-induced shift between the ($\pm^5/_2$, $\pm^3/_2$) and ($\pm^7/_2$, $\pm^5/_2$) transitions is clearly observed in the outer regions of the spectrum. This shift difference is given by[32] $\Delta\nu_{\pm7/2,\pm5/2} - \Delta\nu_{\pm5/2,\pm3/2} = (15/1960)\cdot SOQE^2/\nu_0$, where $SOQE = C_Q(1+\eta^2/3)^{1/2}$ is the socalled second-order quadrupolar effect parameter. From the experimentally observed splitting $\Delta\nu_{\pm7/2,\pm5/2} - \Delta\nu_{\pm5/2,\pm3/2}$ = 1300 ± 50 Hz a value for $SOQE$ = 4.2 ± 0.1 MHz is determined and from the *width of the ssb manifold we obtain* $C_Q \approx 3.8$ *MHz. Combining* these values gives an estimated value for $\eta_Q \approx 0.8$. Employing these data along with approximate parameters for the shielding anisotropy ($\delta_\sigma \approx 270$ ppm and $\eta_\sigma \approx 0.76$, obtained from simulations of the ssb's for the central transition) as starting parameters, an iterative fitting leads to the final parameters listed in Table I. The quality of these parameters is best appreciated by comparison of the simulated ssb spectrum in Figure 4c with the integrated intensity stick-plot spectrum in Figure 4b.

α-$NaVO_3$. Since our commercial sample of sodium metavanadate revealed the presence of the two polymorphs α- and β-$NaVO_3$ as observed from both ^{51}V and ^{23}Na MAS NMR (*vide infra*) we first discuss the MAS NMR spectra obtained for the pure polymorphs synthesized from the commercial sample (see Experimental Section). The MAS NMR spectrum of α-$NaVO_3$ shown in Figure 5a, obtained using a spectral width of 2 MHz and a ^{51}V transmitter frequency, illustrates the ^{51}V (105.15 MHz) as well as the ^{23}Na (105.80 MHz) resonances for α-$NaVO_3$ in the same spectrum. The ssb's from the two ^{23}Na sites do not overlap with the ^{51}V ssb manifold for the employed spinning speed (ν_r = 9.3 kHz), which allow determination of accurate integrated intensities for all ^{51}V ssb's as shown in Figure 5b. Using the procedure described for $LiVO_3$ gives the optimum ^{51}V parameters listed in Table I for α-$NaVO_3$ and the corresponding simulated

(32) Samoson, A. *Chem. Phys. Lett.* **1985**, *119*, 29.

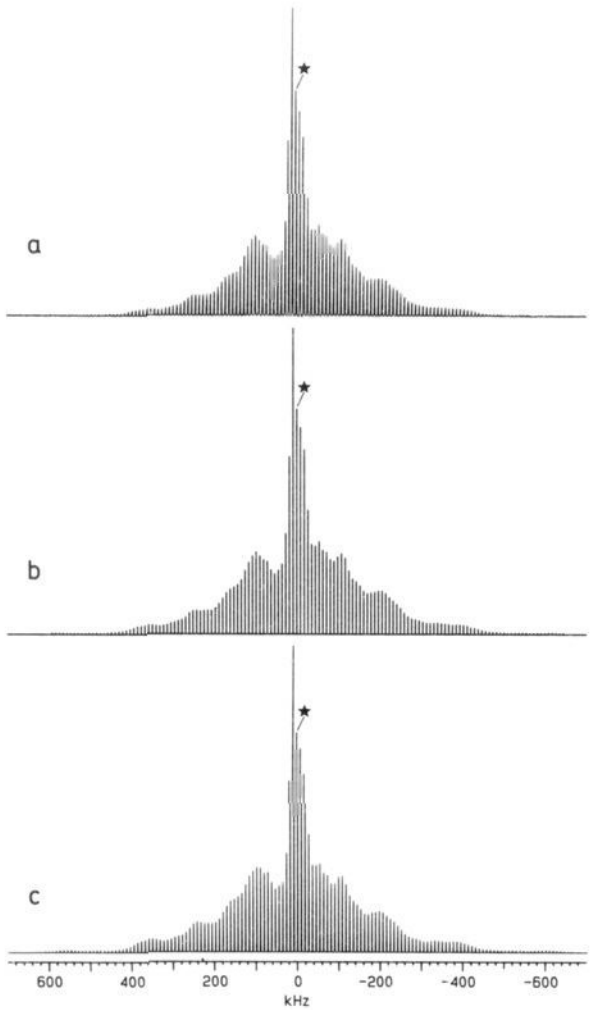

Figure 3. ^{51}V MAS NMR spectrum at 11.7 T (131.4 MHz) of the central and satellite transitions for NH_4VO_3. (a) Experimental spectrum (ν_r = 9.0 kHz). (b) Stick-plot of integrated ssb intensities for the spectrum in part a. (c) Simulated MAS spectrum corresponding to the optimized parameters (Table I) obtained from a seven-parameter fit to the 139 ssb intensities in part b. A Gaussian line width of 900 Hz has been employed for all ssb's in part c. The isotropic peak is marked by an asterisk.

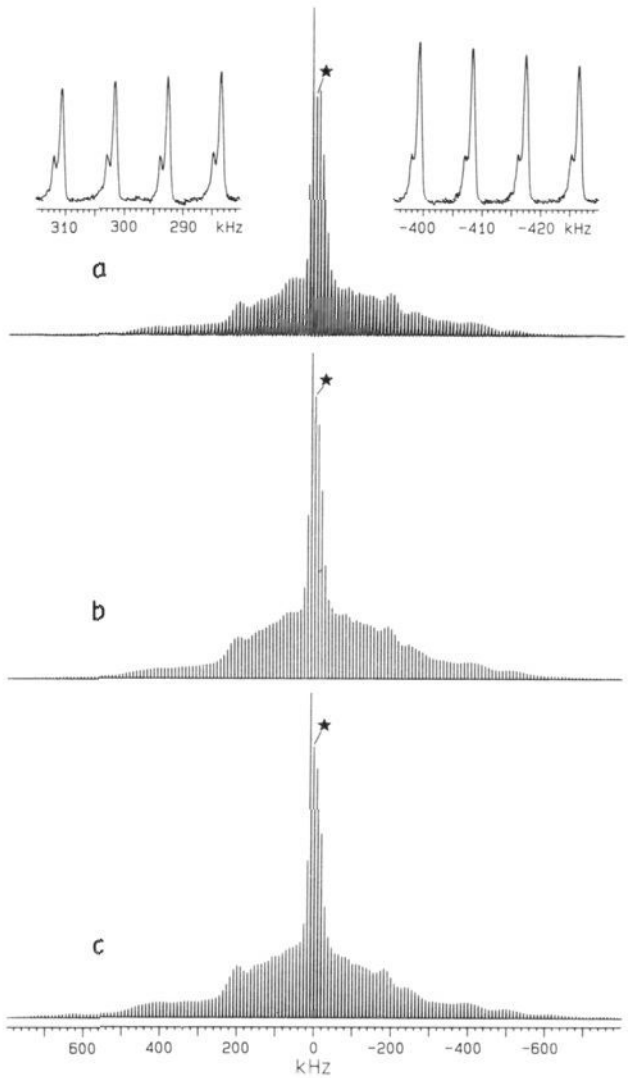

Figure 4. ^{51}V MAS NMR spectrum (105.15 MHz) of the central and satellite transitions for $TlVO_3$. (a) Experimental spectrum (ν_r = 9.1 kHz) where the insets for two regions illustrate the splitting of the ssb's caused by the difference in second-order quadrupolar shift for the ($\pm^5/_2$, $\pm^3/_2$) and ($\pm^7/_2$, $\pm^5/_2$) transitions. (b) Stick-plot of integrated ssb intensities for the spectrum in part a. (c) Simulated MAS NMR spectrum corresponding to the optimized parameters (Table I) resulting from an iterative fitting to the ssb intensities in part b. A Gaussian line width of 900 Hz has been employed for all ssb's in part c. The asterisk indicates the isotropic peak.

spectrum in Figure 5c. The CSA parameters are in good agreement with those determined previously from static-sample NMR of the central transition at high magnetic field[15,17,33] (Table I), however, with a higher accuracy for our MAS NMR data. Mao et al.[19] recently reported quadrupole coupling parameters for α-$NaVO_3$ using NQR (Table I), and the C_Q and η values determined in this study agree within error limits with their data. Quadrupole coupling and CSA data have also been reported from analysis of the static ^{51}V spectrum of the central transition assuming that the principal-axis frames for the CSA and quadrupole tensors coincide.[11] For comparison, a simulated ^{51}V MAS NMR spectrum based on these parameters (Table I)[11] is illustrated in Figure 5d. This spectrum clearly demonstrates that the relative orientation of the two tensors must be considered.

The MAS NMR spectrum in Figure 5a suggests that additional information regarding the structure of α-$NaVO_3$ may be obtained with ^{23}Na MAS NMR. The ^{23}Na MAS NMR spectrum at 7.1 T of the central transitions for the two Na sites in α-$NaVO_3$ is shown in Figure 6b, while Figure 7a illustrates the two sets of overlapping manifolds of ssb's from the satellite transitions at 9.4 T, partly overlapping with the ^{51}V spectrum. The structure of

α-$NaVO_3$ contains two Na atoms in the asymmetric unit, each surrounded by six oxygen atoms.[28] The six coordinated oxygens for the Na(1) site are rather irregularly arranged while the coordination for Na(2) is octahedral to a good approximation.[28] Thus, the ^{23}Na resonance corresponding to the large and small quadrupole coupling is tentatively assigned to Na(1) and Na(2), respectively. For Na(1) the C_Q, η_Q, and δ_{iso} values are most conveniently determined from analysis of the second-order line shape for the central transition giving C_Q = 1.50 ± 0.05 MHz, η_Q = 0.58 ± 0.02, and δ_{iso} = −15.6 ± 0.5 ppm. On the other hand, the singularities, shoulders, and edges of the second-order quadrupolar line shape for the Na(2) site are only partly resolved at 7.1 T (Figure 6b), which impede accurate determination of C_Q and η_Q from the central transition. Examination of the ssb manifold for the satellite transitions (Figure 7a) shows a well-defined shape for the overall ssb envelope, composed of overlapping ssb's from both Na sites. Although the difference in isotropic chemical shifts for Na(1) and Na(2) is ca. 10 ppm (Figure 6b), the second-order quadrupolar shift of the satellite transitions leads

(33) Oldfield, E.; Kinsey, R. A.; Montez, B.; Ray, T.; Smith, K. A. *J. Chem. Soc., Chem. Commun.* **1982**, 254.

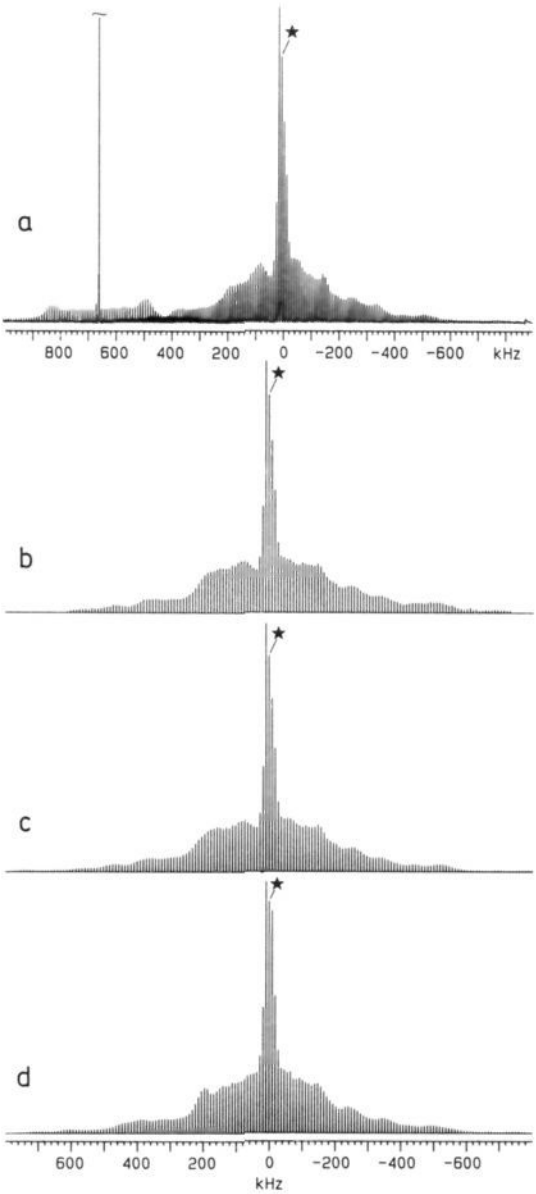

Figure 5. ^{51}V MAS NMR spectrum of the central and satellite transitions at 9.4 T for α-$NaVO_3$. (a) The experimental spectrum (ν_r = 9.3 kHz, 2 MHz spectral width) was recorded with the carrier frequency placed on-resonance for the ^{51}V transitions. The spectrum illustrates the two partially overlapping ssb manifolds from ^{51}V (105.15 MHz) and ^{23}Na (105.80 MHz). (b) Stick-plot of 148 integrated ssb intensities for the ^{51}V ssb manifold in part a. (c and d) Simulated spectra corresponding to (c) the optimized parameters (Table I) from a seven-parameter fit to the ssb intensities in part b and (d) the previously reported data from static powder NMR.[11] A Gaussian line width of 900 Hz has been employed for the simulations. The isotropic peak is marked by an asterisk.

to partly overlapping ssb's for the two Na sites at 9.4 T, independent of the spinning frequency. Quadrupole coupling parameters for Na(2) can be determined from simulations of the experimental ssb envelope, using integrated ssb intensities and including both Na sites. By employing the C_Q and η_Q values for Na(1) (determined from the central transition) and a 1:1 intensity ratio for the two Na sites, fitting of the simulated (summed) to the experimental ssb's gives $C_Q = 0.765 \pm 0.020$ MHz and $\eta_Q = 0.06 \pm 0.02$ for Na(2). The optimum simulated spectrum for the combined set of satellite transitions is shown in Figure 7b, while spectra c and d in Figure 7 display the individual simulated ssb patterns for Na(2) and Na(1), respectively. The C_Q and η_Q values determined for Na(2) are in excellent agreement with the

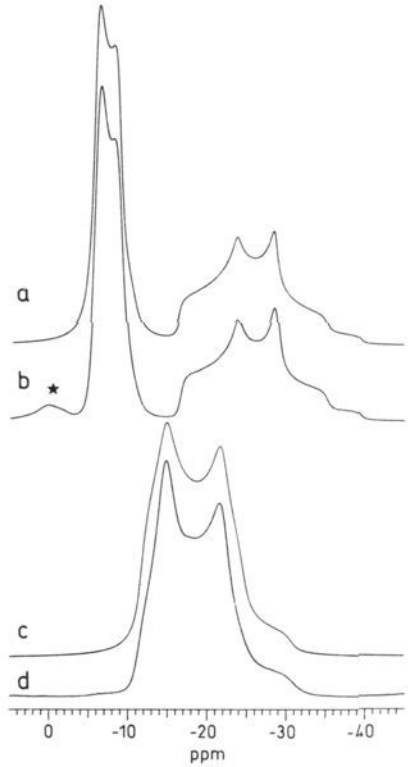

Figure 6. ^{23}Na MAS NMR spectra (7.1 T) of the central transitions for (b) α-$NaVO_3$ and (d) β-$NaVO_3$ (ν_r = 7.2 kHz for both spectra). Optimum simulated lineshapes for the central transitions are shown for the two Na sites in α-$NaVO_3$ (a) and for Na in β-$NaVO_3$ (c) using the parameters given in Table I. The asterisk in part b indicates the centerband of the satellite transitions for the Na(2) site in α-$NaVO_3$.

line shape observed for the central transition at 7.1 T as shown by the simulated line shapes for the two sodium sites in Figure 6a. In a NQR study of α-$NaVO_3$, Mao et al.[19] assumed the broad resonance observed at 782.7 kHz to include a ^{23}Na line. The C_Q and η_Q values for the Na(1) site correspond to a NQR frequency of 791 ± 13 kHz which confirms their assumption. We note that in NQR studies of $I = {}^3/_2$ nuclei (e.g., ^{23}Na) only a single resonance ($\nu = {}^1/_2 C_Q(1 + \eta^2/3)^{1/2}$) is observed which prevents an independent determination of C_Q and η_Q.[34]

β-$NaVO_3$. The 9.4 T ^{51}V MAS NMR spectrum of β-$NaVO_3$ (Figure 8a), the low-temperature polymorph of sodium metavanadate, shows resonances from both ^{51}V and ^{23}Na. The result of a least-squares fitting to the integrated ^{51}V ssb intensities (shown as stick-plot in Figure 8b) gives the ^{51}V data summarized in Table I for β-$NaVO_3$ and the corresponding simulated spectrum in Figure 8c. We note that for $\eta_\sigma = 0$ the angle ψ becomes undefined. The ^{51}V central transition in β-$NaVO_3$ has recently been studied by static and MAS NMR[17] leading to a determination of the CSA and isotropic shift parameters. These values are in good agreement with those obtained in this study considering the error limits and the correction of the chemical shift for the second-order quadrupolar shift determined here.

The environments of the sodium ion in β-$NaVO_3$ can be probed by ^{23}Na MAS NMR as illustrated by the ^{23}Na spectra of the central transition (7.1 T) and the satellite transitions (9.4 T) in Figures 6d and 9a, respectively. Both ^{23}Na MAS NMR spectra demonstrate that the structure of β-$NaVO_3$ contains only one Na site in the asymmetric unit in agreement with the reported crystal structure from XRD.[29] Obviously, for this sample the ^{23}Na quadrupole coupling parameters may be determined by simulation of the lineshape for the central transition (Figure 6d); however, it is our experience that generally a considerable higher accuracy

(34) Gravina, S. J.; Bray, P. J.; *J. Magn. Reson.* **1990**, *89*, 515.

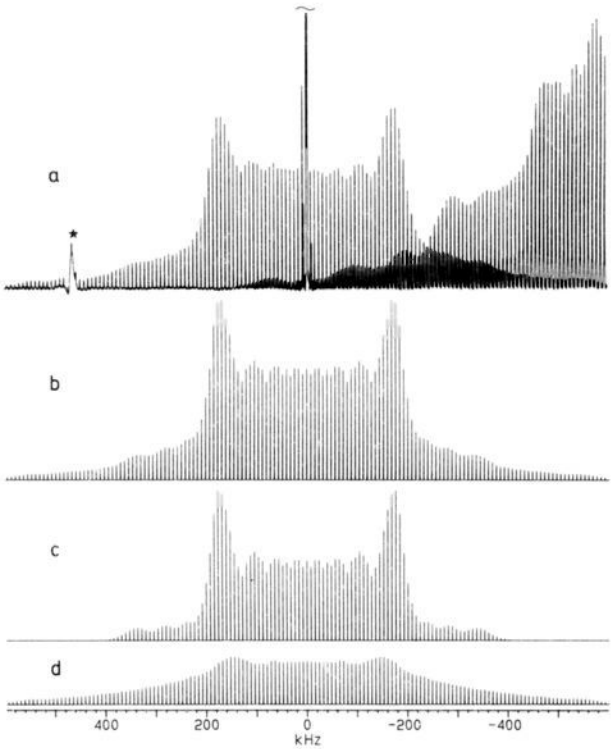

Figure 7. ^{23}Na MAS NMR spectrum (9.4 T) of the satellite transitions for α-$NaVO_3$. (a) Experimental spectrum (ν_r = 8.0 kHz) showing the two sets of ssb manifolds from the two Na sites in α-$NaVO_3$ (almost completely overlapping by coincidence; see text) which partly overlap into the ^{51}V spectrum at lower frequency. (b) Optimum simulated spectrum of the two overlapping manifolds of ssb's obtained using an intensity ratio of 1:1 and the C_Q and η_Q values for Na(1) and Na(2) in Table I. Simulated spectra of the satellite transitions for the individual Na sites are shown for Na(2) (c) (C_Q = 0.765 MHz, η_Q = 0.06) and for Na(1) (d) (C_Q = 1.50 MHz, η_Q = 0.58). The simulated spectra employed Gaussian linewidths of 400 and 550 Hz for the ssb's from Na(2) and Na(1), respectively. The asterisk indicates the ^{63}Cu resonance from the rf copper coil.

for the parameters is achieved by fitting the intensities of the observed ssb manifold for the satellite transitions. This procedure gives C_Q = 1.42 ± 0.02 MHz and η_Q = 0.27 ± 0.02. The quality of the optimized parameters is illustrated by the simulations of the ssb manifold (Figure 9b) and the lineshape for the central transition (Figure 6c). A distinct variation in quadrupole coupling parameters and isotropic chemical shifts is observed for α- and β-$NaVO_3$ (Table I), indicating that a considerable structural change of the Na environments is involved in the irreversible phase transition from β- to α-$NaVO_3$ at 405 °C.[23]

Commercial Sample of a Mixture of α- and β-$NaVO_3$. The differences in the ^{23}Na C_Q, η_Q, and δ_{iso} parameters for α- and β-$NaVO_3$ allow a clear discrimination and quantification of the two polymorphs in a mixture as illustrated by the ^{23}Na MAS NMR spectra of the central transitions for a commercial sample of sodium metavanadate at 9.4 (Figure 10b) and 7.1 T (Figure 10d). At both magnetic fields the ^{23}Na lineshapes of the centerbands for the central transition in β-$NaVO_3$ and for Na(1) in α-$NaVO_3$ overlap. However, at 9.4 T four distinct singularities are clearly observed for the two overlapping centerbands. Deconvolution of the ^{23}Na MAS NMR spectra at 7.1 and 9.4 T, employing lineshapes for the central transitions corresponding to C_Q, η_Q, and δ_{iso} (Table I) determined for the individual polymorphs, leads to a quantitative determination of α- and β-$NaVO_3$ for our commercial sample. For both deconvoluted spectra in Figure 10 an intensity ratio of $I(\alpha\text{-}NaVO_3)/I(\beta\text{-}NaVO_3)$ = 2.15 ± 0.15 is obtained, where $I(\alpha\text{-}NaVO_3)$ includes the intensities for the Na-

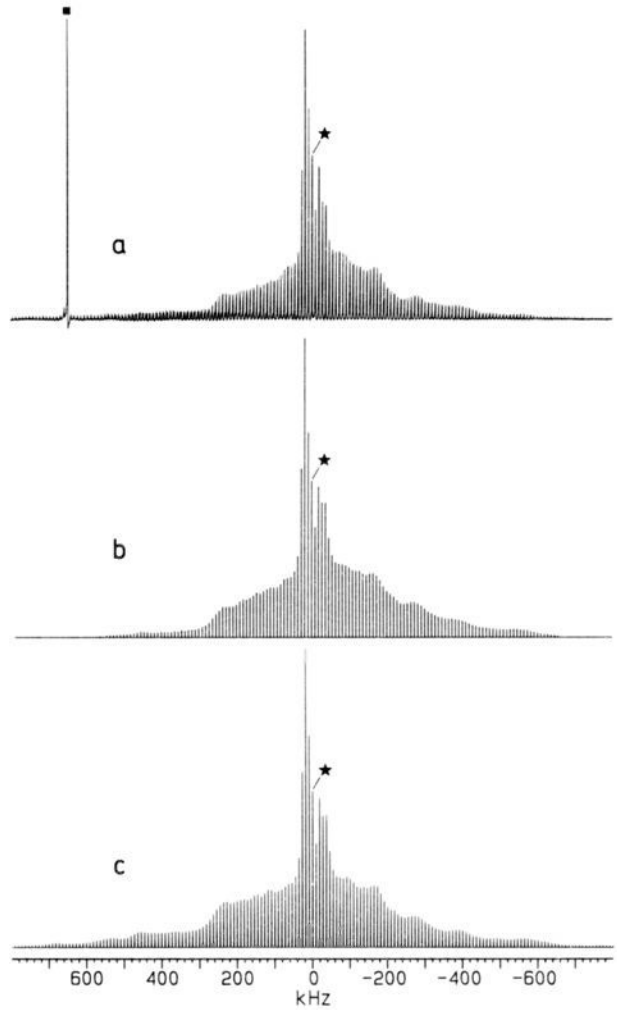

Figure 8. ^{51}V MAS NMR spectrum (9.4 T) of the central and satellite transitions for β-$NaVO_3$. (a) Experimental spectrum (ν_r = 9.1 kHz) illustrating the overlapping manifolds of ssb's from the ^{51}V (105.15 MHz) and ^{23}Na (105.80 MHz) spectra. (b) Stick-plot of integrated ssb intensities for the ^{51}V ssb manifold in part a. (c) Optimum simulated spectrum of the ssb's in part b corresponding to the ^{51}V parameters in Table I. A Gaussian line width of 1000 Hz is employed for all ssb's in part c. The isotropic ^{51}V peak is indicated by an asterisk while the solid square marks the central transition in the ^{23}Na spectrum.

(1) and Na(2) site. This ratio gives a composition of 68 ± 2% α-$NaVO_3$ and 32 ± 2% β-$NaVO_3$ for the sample.

Alternatively, the mixture of the two polymorphs in our sample can be distinguished using ^{51}V MAS NMR as illustrated by the 9.4 T spectrum, employing ν_r = 9.2 kHz, in Figure 11a. Under these experimental conditions the spectrum shows two well-separated manifolds of ssb's, which are easily assigned to α- and β-$NaVO_3$ by comparison with the ^{51}V MAS NMR spectra of the individual components shown in Figures 5 and 8. A simulated spectrum of the overlapping manifolds of ssb's is shown in Figure 11b which is based on the ^{51}V data for α- and β-$NaVO_3$ (Table I) and the ^{51}V intensity ratio of $I(\alpha\text{-}NaVO_3)/I(\beta\text{-}NaVO_3)$ = 1.9 ± 0.2 as determined from a comparison of simulated and experimental integrated ssb intensities for the two ssb manifolds. The intensity ratio, obtained from the ^{51}V MAS spectrum, corresponds to a composition of 66 ± 3% α-$NaVO_3$ and 34 ± 3% β-$NaVO_3$ for the sample, which is in good agreement with the results obtained above from the ^{23}Na MAS NMR spectra.

KV_3O_8. As the final example, the ^{51}V MAS NMR spectrum (9.4 T, ν_r = 9.2 kHz) of KV_3O_8 in Figure 12a illustrates the applicability of the MAS method for determination of CSA and quadrupole coupling parameters in a sample with more than one

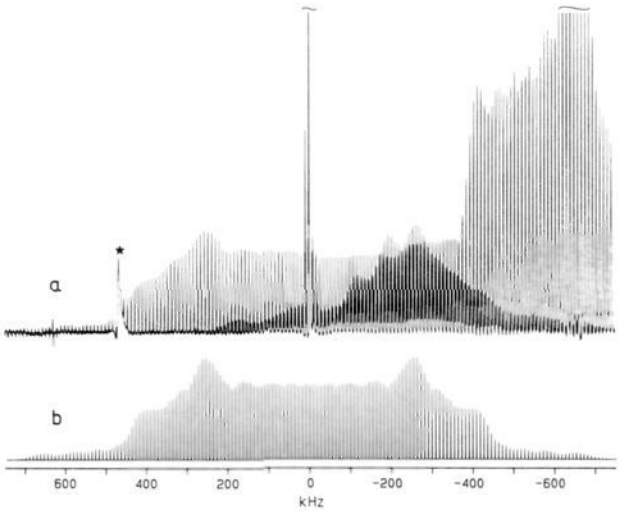

Figure 9. ^{23}Na MAS NMR spectrum (9.4 T) of the satellite transitions for β-$NaVO_3$. (a) Experimental spectrum (ν_r = 9.1 kHz) showing a partial overlap of the manifold of ssb's from ^{23}Na into the ^{51}V spectrum at lower frequency. (b) Optimum simulated spectrum corresponding to C_Q = 1.42 MHz, η_Q = 0.27, and a Gaussian line width of 800 Hz for the ssb's. The asterisk indicates the ^{63}Cu resonance from the rf copper coil.

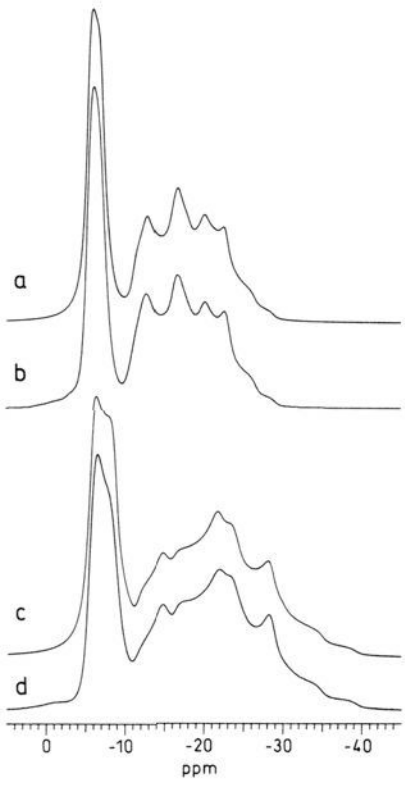

Figure 10. ^{23}Na MAS NMR spectra of the central transitions for a commercial sample of sodium metavanadate obtained at (b) 9.4 T (ν_r = 7.4 kHz) and (d) 7.1 T (ν_r = 7.2 kHz). Parts a and c illustrate optimum simulated spectra for the central transitions at 9.4 and 7.1 T, respectively. The simulated spectra employed the ^{23}Na data for α- and β-$NaVO_3$ in Table I and an intensity ratio of $I(\alpha\text{-}NaVO_3)/I(\beta\text{-}NaVO_3)$ = 2.15 corresponding to a composition of 32% β-$NaVO_3$ and 68% α-$NaVO_3$ for the sample.

vanadium site in the asymmetric unit. KV_3O_8, a potential electrode material for rechargeable solid-state sodium and lithium cells,[24] contains sheets of edge-sharing VO_6 octahedra with two nonequivalent vanadium sites, V(1) and V(2), in the asymmetric unit and in the ratio of 1:2, respectively.[30] Thus, the observation of two overlapping manifolds of ssb's in the ^{51}V MAS NMR spectrum is in accordance with the reported crystal structure.[30] The two manifolds are well-separated, and integrated ssb intensities for each V site can be accurately determined as illustrated by the stick-plots for the V(1) and V(2) site in Figures 12b and 13b, respectively. ^{51}V parameters for the quadrupole and shielding interactions are obtained using the optimization procedure described above and are summarized in Table I. The corresponding simulated manifolds of ssb's for V(1) and V(2) (Figures 12c and 13c) are in excellent agreement with the experimental ssb intensities. A simulated spectrum which includes both ssb manifolds in an intensity ratio of 1:2 for V(1) and V(2), respectively, and second-order quadrupolar shifts for all transitions is shown in Figure 13a. Comparison of this spectrum with the experimental spectrum in Figure 12a demonstrates the high performance of the method.

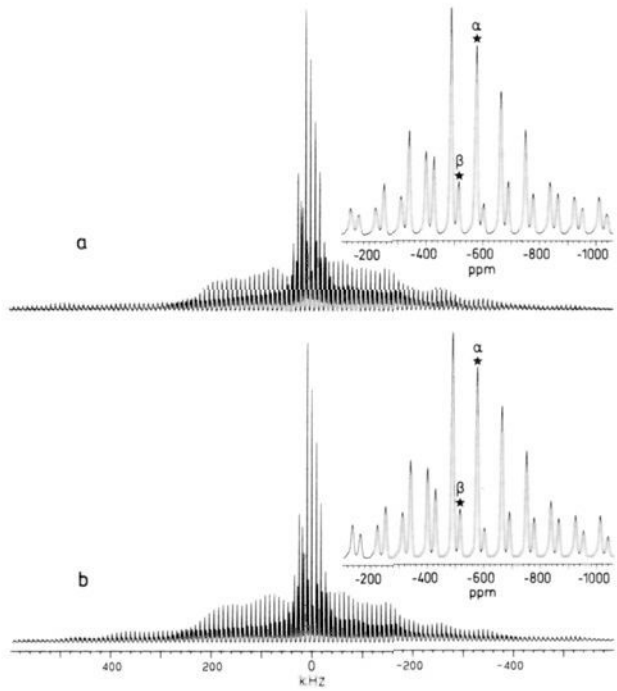

Figure 11. (a) ^{51}V MAS NMR spectrum (9.4 T, ν_r = 9.2 kHz) of a commercial sample of sodium metavanadate illustrating the overlapping manifolds of ssb's from ^{51}V in α- and β-$NaVO_3$. The region for the central transitions is shown in the inset, where α and β indicate the centerbands for the two $NaVO_3$ polymorphs. (b) Simulated spectrum of the ssb manifolds in part a employing the ^{51}V parameters for α- and β-$NaVO_3$ shown in Table I and an intensity ratio of $I(\alpha\text{-}NaVO_3)/I(\beta\text{-}NaVO_3)$ = 1.9, corresponding to a composition of 34% β-$NaVO_3$ and 66% α-$NaVO_3$ for the sample, as determined from a comparison of simulated and experimental ssb intensities for the two manifolds. The simulated spectrum employs Gaussian line widths of 1000 ($^1/_2$, $^{-1}/_2$), 1100 ($\pm^3/_2$, $\pm^1/_2$), 1200 ($\pm^5/_2$, $\pm^3/_2$), and 1500 Hz ($\pm^7/_2$, $\pm^5/_2$) for the ssb's from the individual transitions for α- and β-$NaVO_3$ and also includes second-order quadrupolar shifts for all transitions.

Relationships of the ^{51}V NMR Parameters with Structural Data. Although the XRD results show that KVO_3, NH_4VO_3, and $TlVO_3$ are isomorphous,[25,26] considerable variations in the ^{51}V quadrupole coupling parameters, which are, however, somewhat smaller for the CSA, are observed for these vanadates (Table I). C_Q is proportional to the principal element (V_{zz}) of the EFG tensor and it has been proposed[35,36] that the geometrical dependence of the EFG tensor can be approximated by the simple relation

$$V' = \frac{e}{4\pi\epsilon_0}\sum_{i=1}^{4}\nabla\nabla\mathbf{R}_i^{-1} \qquad (6)$$

where $\mathbf{R}_i$ is the modulus of the internuclear vector between the

(35) Cohen, M. H.; Reif, F. *Solid State Phys.* **1957**, *5*, 321.
(36) Villa, M.; Bjorkstam, J. L. *J. Magn. Reson.* **1983**, *51*, 349.

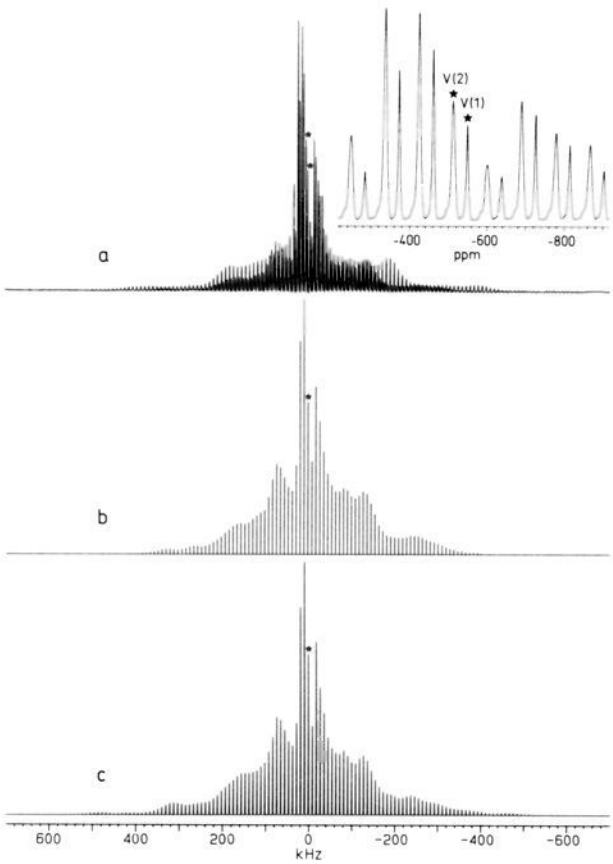

Figure 12. ^{51}V MAS NMR spectrum of the central and satellite transitions for KV_3O_8. (a) Experimental spectrum (ν_r = 9.2 kHz) illustrating the overlapping manifolds of ssb's from the two ^{51}V sites in KV_3O_8. The inset illustrates the region for the central transitions. (b) Stick-plot of integrated ssb intensities for V(1). (c) Simulated ssb manifolds corresponding to the optimized parameters (Table I) for the V(1) site. A Gaussian line width of 1000 Hz has been employed for the ssb's in part c. The centerbands are marked by asterisks. ^{51}V MAS NMR spectra of the V(2) site and a simulated spectrum of the ssb manifolds from both V sites are shown in Figure 13.

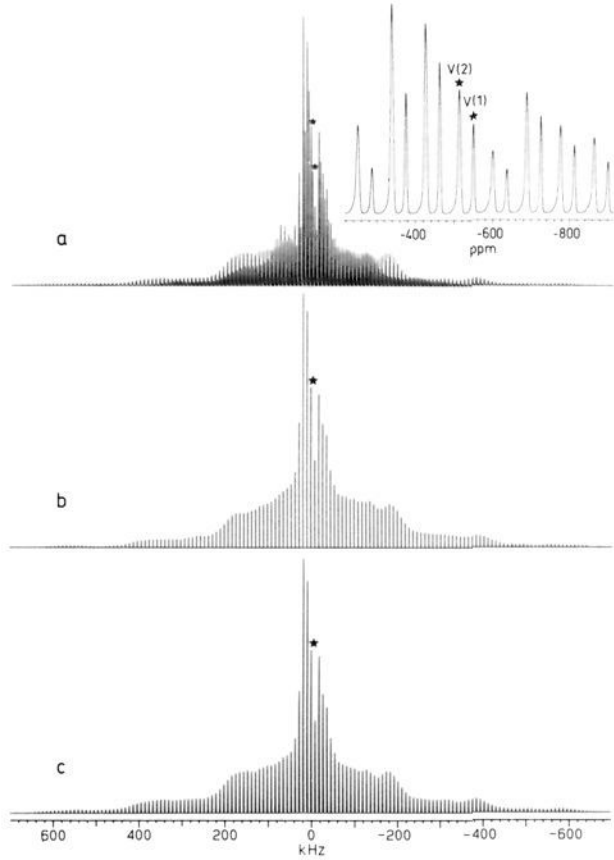

Figure 13. (a) Simulated ^{51}V MAS NMR spectrum (105.15 MHz, ν_r = 9.2 kHz) of the ssb manifolds for the two V sites in KV_3O_8 obtained using the ^{51}V parameters in Table I and an intensity ratio of 1:2 for V(1) and V(2), respectively. The simulated spectrum and inset in part a should be compared with the experimental ^{51}V MAS NMR spectrum of KV_3O_8 in Figure 12a. The simulated spectrum employs Gaussian line widths of 700 ($^1/_2$, $-^1/_2$), 800 ($\pm^3/_2$, $\pm^1/_2$), 1200 ($\pm^5/_2$, $\pm^3/_2$), and 1500 Hz ($\pm^7/_2$, $\pm^5/_2$) for the ssb's from the individual transitions for both V sites and also includes second-order quadrupolar shifts for all transitions. (b) Stick-plot of experimental integrated ssb intensities for V(2) in KV_3O_8 as determined from the ^{51}V MAS NMR spectrum in Figure 12a. (c) Simulated spectrum of the ssb's in part b corresponding to the optimized parameters for V(2) shown in Table I and using a Gaussian line width of 1000 Hz for the ssb's. The centerbands are indicated by asterisks.

quadrupole nucleus and the O_i oxygen atom. This relation considers atoms only within the first coordination sphere and has recently proven useful in the assignment of ^{27}Al quadrupole coupling constants for AlO_4 tetrahedra in calcium aluminates.[37] Employing eq 6 to the VO_4 tetrahedra for the three isomorphous metavanadates along with atomic coordinates from the refined crystal structures[38] yields the following values (after diagonalization of V') for the principal element V'_{zz} ($\times 10^{20}$ V m^{-2}): 1.76 (NH_4VO_3), 2.24 ($TlVO_3$), and 2.34 (KVO_3). Thus, the predicted order of increasing V'_{zz} values ($NH_4VO_3 < TlVO_3 < KVO_3$) corresponds to the increasing order for the experimental C_Q values (Table I). Furthermore, it is seen that the CSA (i.e., $\delta_\sigma = \sigma_{zz} - \sigma_{iso}$) for these compounds increases in the same order as observed for the C_Q values and shows an excellent correlation with these data (however, only three points are used). This might suggest that the axes for the principal element (λ_{zz}) of the EFG and CSA tensors are almost parallel which is fully supported by the relative orientation of the two tensors, i.e., small χ angles, determined experimentally for KVO_3, NH_4VO_3, and $TlVO_3$ (Table I). For these isomorphous metavanadates the symmetry of the orthorhombic crystal lattice (*Pcbm*)[25,26] shows that the two V–O bonds, constituting the chains of VO_4 tetrahedra, are identical while the bond lengths for the two nonbridging V–O bonds differ by less than 1%.[38] Thus, the symmetry of the VO_4 tetrahedra is close to C_{2v} since all O–V–O bond angles deviate only slightly from the ideal tetrahedral angle (109.47°). From model calculations of the geometrical dependence of the EFG tensor, employing eq 6 and under the condition of *ideal* C_{2v} symmetry for the geometry of the VO_4 tetrahedra, we obtain an EFG asymmetry parameter of $\eta'_Q = 1.0$ for two cases: (a) all O–V–O bond angles are exact tetrahedral and the bond lengths are pairwise identical (obviously excluding the ideal tetrahedron where η_Q is undefined) and (b) all V–O bond lengths are equal but the O–V–O angles deviate from the tetrahedral value. However, for other cases of exact C_{2v} symmetry for a VO_4 unit with non-ideal tetrahedral O–V–O bond angles as well as pairwise identical V–O bond lengths, calculations show that η'_Q becomes less than 1.0 and appears to be sensitive to even small variations in these structural parameters. Model calculations for KVO_3, NH_4VO_3, and $TlVO_3$ using the actual bond lengths[38] but assuming the *ideal* tetrahedral value for the O–V–O bond angles give $\eta'_Q = 1.0$ for all three metavanadates. This might suggest that the experimental η_Q values for KVO_3, NH_4VO_3, and $TlVO_3$, which are considerably lower than 1.0 (Table I), reflect deviations in the O–V–O bond angles from the perfect tetrahedral value rather than variations in the V–O bond lengths. However, further calculations show that it is rather a

(37) Skibsted, J.; Henderson, E.; Jakobsen, H. J. *Inorg. Chem.* **1993**, *32*, 1013.

(38) Hawthorne, F. C.; Calvo, C. *J. Solid State Chem.* **1977**, *22*, 157.

combination of changes in both bond angles and lengths that makes η_Q extremely sensitive to the tetrahedral geometry. Calculations of η'_Q for KVO_3, NH_4VO_3, and $TlVO_3$, employing the actual O–V–O bond angles and V–O bond lengths determined from the refined crystal structures,[38] give $\eta'_Q = 0.49$ (KVO_3), $\eta'_Q = 0.40$ (NH_4VO_3), and $\eta'_Q = 0.80$ ($TlVO_3$), which agree fairly well with the η_Q values determined experimentally (at least for NH_4VO_3 and $TlVO_3$, Table I) and also reflect the sensitivity of η'_Q to the VO_4 geometry. We note that asymmetry parameters close to 1.0 for the ^{27}Al quadrupole coupling tensor have recently been reported from ^{27}Al MAS NMR studies of AlO_4 tetrahedra in chain structures and used as an argument for C_{2v} aluminum symmetry of these AlO_4 units.[39] ^{31}P shielding anisotropies and the individual tensor elements determined from solid-state NMR studies of phosphates have previously been shown to correlate with structural parameters such as P–O bond lengths, O–P–O bond angles, and the average deviation of the O–P–O bond angles from perfect tetrahedral symmetry.[40,41] Corresponding correlations between the ^{51}V shielding anisotropies (or the individual tensor elements) and similar structural parameters for the VO_4 tetrahedra are not apparent from the data for the metavanadates (Table I). For the CSA asymmetry parameters (η_σ) in Table I and those reported for $CsVO_3$ ($\eta_\sigma = 0.61$) and $RbVO_3$ ($\eta_\sigma = 0.71$),[17] it is observed that this parameter varies only slightly within the series of metavanadates. From these values and CSA asymmetry parameters for other tetrahedrally-coordinated vanadium compounds,[15] it appears that $\eta_\sigma = 0.7 \pm 0.1$ is characteristic for VO_4 tetrahedra in chain structures (i.e., Q^2 units).

The structural similarities of the two isomorphs α-$NaVO_3$ and $LiVO_3$[27,28] are also reflected by the eight ^{51}V parameters describing the magnitudes and relative orientation of the quadrupole coupling and CSA tensors. Employing the symmetry relations in eq 4 it is observed that, within the error limits for the Euler angles (ψ,χ,ξ) (Table I), the relative orientation of the two tensors is identical for these compounds. Furthermore, the axis for the principal element (λ_{zz}) of the EFG and CSA tensors almost coincides (indicated by the small value for the angle χ) for the two compounds. In addition, $LiVO_3$ and α-$NaVO_3$ exhibit nearly identical η_σ and δ_{iso} values while somewhat larger variations are observed for C_Q, η_Q, and δ_σ. From the crystal structure data of the VO_4 tetrahedra[27,28] and employing eq 6 we estimate the following values for the geometrical dependence of the EFG tensor for the two compounds: $V'_{zz} = 1.56 \times 10^{20}$ V m^{-2} ($LiVO_3$) and $V'_{zz} = 1.69 \times 10^{20}$ V m^{-2} (α-$NaVO_3$). Qualitatively these V'_{zz} values are in accord with the somewhat larger C_Q value observed for α-$NaVO_3$. Furthermore, α-$NaVO_3$ also exhibits the larger δ_σ value of the two compounds. Thus, the C_Q and δ_σ values for $LiVO_3$ and α-$NaVO_3$ show the same relationship as observed within the series of the isomorphous NH_4^+, Tl^+, and K^+ metavanadates. Although the VO_4 tetrahedra in $LiVO_3$ and α-$NaVO_3$ each have four different V–O bond lengths and all O–V–O bond angles deviate from the perfect tetrahedral value, the calculated EFG tensors, corresponding to the geometrical dependence expressed by eq 6, lead to the same value for the estimated asymmetry parameter $\eta'_Q = 0.91$ for the two compounds. This value of η'_Q is in good agreement with the quadrupole coupling asymmetry parameter for $LiVO_3$ (Table I) but deviates somewhat from the η_Q value determined for α-$NaVO_3$. Examination of the individual V–O bond lengths and O–V–O bond angles in $LiVO_3$ and α-$NaVO_3$ shows very small variations in these parameters (i.e., the mean values for the numerical difference in V–O bond lengths and O–V–O bond angles are 0.009 Å and 1.2°, respectively) which leads to the same calculated η'_Q value (eq 6) for the two compounds. Thus, we presume that the difference between the estimated (η'_Q) and experimental (η_Q) values for the asymmetry parameter in α-$NaVO_3$ is caused by contributions to the EFG tensor from ions outside the first coordination sphere.

The structure of β-$NaVO_3$[29] is quite different from the tetrahedral structures of the other metavandates, which is also reflected by the ^{51}V parameters (Table I). In β-$NaVO_3$ the vanadium atom is coordinated to five oxygens in a distorted trigonal bipyramid which forms a double-linked chain structure.[29] From the CSA and δ_{iso} parameters it is evaluated that of all the metavanadates β-$NaVO_3$ possesses the most deshielded (σ_{xx} = 211 ppm) and most shielded (σ_{zz} = 1022 ppm) CSA tensor element. CSA parameters of similar magnitude to those for β-$NaVO_3$ have recently been reported for ^{51}V in V_2O_5 ($\delta_\sigma = 645$ ppm, $\eta_\sigma = 0.11$, $\delta_{iso} = -614.3$ ppm; i.e., $\sigma_{xx} = 256$ ppm and $\sigma_{zz} = 1259$ ppm) in our preliminary investigation on ^{51}V MAS NMR.[10] The vanadium atom in V_2O_5 is bonded to five oxygens in a trigonal bipyramid;[42] however, the coordination to the oxygens is sometimes referred to as being that of a distorted octahedron (or a square-bipyramid) because of the presence of an additionally and exceptionally long V–O "bond" (2.785 Å) in the opposite direction of the shortest V–O bond.[18,42] The symmetry of the VO_5 unit in β-$NaVO_3$ is similar to that of the trigonal bipyramid in V_2O_5, since the base of the pyramid forms a mirror plane in both polyhedra.[29,42] V_2O_5 has previously been studied by ^{51}V single-crystal NMR[18] which shows that the most deshielded element of the CSA tensor (σ_{xx}) is orthogonal to the mirror plane and the unique element (σ_{zz}) is oriented along the shortest V–O bond in the base of the trigonal pyramid. The mirror-plane symmetry of the VO_5 units for both V_2O_5 and β-$NaVO_3$ would indicate a similar orientation of the shielding tensor elements in β-$NaVO_3$ and V_2O_5. Thus, we tentatively suggest that σ_{xx} for β-$NaVO_3$ is orthogonal to the mirror plane, i.e., σ_{yy} and σ_{zz} are in the basal plane of the trigonal bipyramid, and σ_{zz} is oriented along the shortest V–O bond. Obviously, an unambigous establishment of the orientation of the CSA tensor in β-$NaVO_3$ will have to await the result of a single-crystal ^{51}V NMR study. However, we note that with this orientation of the shielding tensors in V_2O_5 and β-$NaVO_3$, the most shielded element (σ_{zz}, the unique tensor element) is almost perpendicular to a pseudoplane containing the longest V–O bonds. This observation is similar to the results obtained from solid-state ^{113}Cd NMR demonstrating that long Cd–O bonds lead to anomalously large shielding of a tensor element perpendicular to such bonds.[43]

For KV_3O_8 the oxygen coordination for both V(1) and V(2) has been characterized as a square bipyramid, where the oxygens outside the base of the pyramid have the shortest and longest V–O bond lengths.[30] V(2) has the most distorted environments which is clearly reflected by the variations in the V–O bond lengths and in the mean deviation (D) of the twelve O–V–O bond angles from perfect octahedral symmetry. For both V sites the shortest V–O bond length is 1.58 Å while a considerable difference in the longest bond length for the two sites is observed ($d_{V(1)-O} = 2.18$ Å, $d_{V(2)-O} = 2.91$ Å).[30] The mean angular deviation from perfect symmetry for the $VO_6(1)$ and $VO_6(2)$ unit is $D = 8.1°$ and 13.9°, respectively. Recent molecular orbital calculations of the ^{95}Mo EFG's for $[MoO_6]^{6-}$ units have shown that bond-angle as well as bond-length variations within the first coordination sphere also for *octahedral* coordination contribute significantly to the magnitude of the quadrupole coupling constant.[1] Thus, the larger quadrupole coupling constant (C_Q) for the V(2) site compared to V(1), as determined from the ^{51}V MAS NMR spectrum, agrees with the above structural considerations. Furthermore, V(2) exhibits the larger shielding anisotropy of the two V sites in

(39) Dec, S. F.; Maciel, G. E.; Fitzgerald, J. J. *J. Am. Chem. Soc.* **1990**, *112*, 9069.
(40) Turner, G. L.; Smith, K. A.; Kirkpatrick, R. J.; Oldfield, E. *J. Magn. Reson.* **1986**, *70*, 408.
(41) Un, S.; Klein, M. P. *J. Am. Chem. Soc.* **1989**, *111*, 5119.
(42) Bachmann, H. G.; Ahmed, F. R.; Barnes, W. H. *Z. Kristallogr.* **1961**, *115*, 110.
(43) Honkonen, R. S.; Ellis, P. D. *J. Am. Chem. Soc.* **1984**, *106*, 5488. Kennedy, M. A.; Ellis, P. D.; Jakobsen, H. J. *Inorg. Chem.* **1990**, *29*, 550.

agreement with the correlation between C_Q and δ_σ observed for the metavanadates. The oxygen coordination within the two VO_6 units in KV_3O_8 (especially for the V(2) site) is similar to the coordination in V_2O_5, referred to as a square bipyramid when the anomalously long V–O bond in V_2O_5 is taken into account.[18,30,42] As discussed for β-$NaVO_3$, the most shielded and unique element (σ_{zz}) for V_2O_5 is oriented along the shortest V–O bond,[18] i.e., along the pseudo 4-fold rotation axis. Thus, we predict the most shielded and unique element (σ_{zz}) for both the V(1) and V(2) sites in KV_3O_8 to be oriented along the shortest V–O bond (1.58 Å) of the two VO_6 units, i.e., along the pseudo 4-fold axis. We note that the predicted direction of the unique elements for the two CSA tensors along the pseudo 4-fold axis in the VO_6 units is in accordance with the experimental value $\eta_\sigma \approx 0$ (i.e., $\sigma_{xx} \approx \sigma_{yy}$ with both elements in the pseudoplane of the square bipyramids and most likely with their axes oriented toward the oxygen atom corners).

It is clear that the ^{51}V quadrupole coupling and CSA parameters determined in this study contain more information about the ^{51}V environments in the vanadates than discussed in this section. A more detailed understanding of the experimental ^{51}V parameters will have to await molecular orbital calculations of ^{51}V EFG and CSA tensors.

Conclusions

This work has demonstrated that all parameters describing the magnitudes and relative orientation of the quadrupole and shielding tensors for a quadrupolar nucleus can be determined from the manifold of spinning sidebands (ssb's) observed in the MAS spectrum for the central *and* satellite transitions. Computer simulations combined with least-squares optimization of the ssb intensities from all seven ^{51}V transitions for a series of metavanadates and KV_3O_8 have led to a determination of accurate ^{51}V parameters for these compounds. Compared to previously reported CSA data for some of the samples, obtained from static powder NMR spectra of the ^{51}V central transition at high magnetic field strengths,[15,17,33] the CSA parameters determined from the ^{51}V MAS NMR spectra in this study are of considerably higher accuracy. The quadrupole coupling parameters determined in this work for KVO_3, α-$NaVO_3$, and NH_4VO_3 are in excellent agreement with those recently reported from a NQR study by Mao et al.[19] The ability to determine CSA parameters, C_Q, η_Q, and the relative orientation of the quadrupole coupling and shielding tensors from a single experiment makes MAS NMR a superior method compared to NQR for characterization of the local environments for the ^{51}V nucleus in vanadium compounds. Thus, the comment by Mao *et al.*,[19] concerning the usefulness of solid-state NMR methods, should be reconsidered in light of the results achieved in this study. Relationships between the ^{51}V NMR parameters and structural data are observed and discussed. Thus, correlations between the quadrupole coupling constant (C_Q) and the shielding anisotropy (δ_σ) as well as between C_Q and the geometry of the VO_4 tetrahedra are observed within the two series of isomorphous metavanadates, i.e., KVO_3, NH_4VO_3, and $TlVO_3$ on one hand and $LiVO_3$ and α-$NaVO_3$ on the other. Finally, the ^{51}V quadrupole coupling and CSA parameters determined from the present (and possible future) ^{51}V MAS NMR studies should form the experimental basis for initiating and testing molecular orbital calculations of ^{51}V EFG and CSA tensors and thereby contribute to an improved insight into the electronic and geometric structure of vanadium compounds.

Acknowledgment. The use of the facilities at the University of Aarhus NMR Laboratory, sponsored by Teknologistyrelsen, the Danish Research Councils (SNF and STVF), Carlsbergfondet, and Direktør Ib Henriksens Fond, is acknowledged. J.S. thanks SNF (11-9160) for financial support. We thank Aarhus University Research Foundation for equipment grants. We are grateful to Dr. K. West (Technical University of Denmark, Copenhagen, Denmark) for providing the sample of KV_3O_8 and to Dr. A. N. Christensen (Department of Chemistry, Aarhus University, Denmark) for his help in the synthesis of $LiVO_3$, $TlVO_3$, and β-$NaVO_3$.

Registry numbers supplied by author: $LiVO_3$: 15060-59-0; KVO_3: 13769-43-2; NH_4VO_3: 7803-55-6; $NaVO_3$: 13718-26-8; $TlVO_3$: 13453-47-9; KV_3O_8: 12056-32-5.